Dalton Transactions

A new family of anti-perovskite oxyhydrides with tetrahedral GaO_4 polyanions

Journal:	*Dalton Transactions*
Manuscript ID	DT-ART-05-2023-001555.R1
Article Type:	Paper
Date Submitted by the Author:	09-Jun-2023

Complete List of Authors:	Ayu, Nur Ika Puji; High Energy Accelerator Research Organization; SOKENDAI Takeiri, Fumitaka; SOKENDAI, Department of Materials Molecular Science; Institute for Molecular Science; PRESTO; RIKEN Ogawa, Takafumi; Japan Fine Ceramics Center, Nanostructures Research Laboratory Kuwabara, Akihide; Japan Fine Ceramics Center, Nanostructures Research Laboratory Hagihala, Masato; High Energy Accelerator Research Organization; SOKENDAI Saito, Takashi; High Energy Accelerator Research Organization, Institute of Materials Structure Science; SOKENDAI Kamiyama, Takashi ; High Energy Accelerator Research Organization; SOKENDAI; Institute of High Energy Physics Chinese Academy of Sciences; China Spallation Neutron Source Kobayashi, Genki; RIKEN, Cluster for Pioneering Research; Institute for Molecular Science; SOKENDAI

A new family of anti-perovskite oxyhydrides with tetrahedral GaO_4 polyanions

cafaReceived 00th January 20xx,
Accepted 00th January 20xx

DOI: 10.1039/x0xx00000x

Nur Ika Puji Ayu,[ab] Fumitaka Takeiri,*[bcde] Takafumi Ogawa,[f] Akihide Kuwabara,[f] Masato Hagihala,[ab] Takashi Saito,[ab] Takashi Kamiyama,[abgh] Genki Kobayashi*[bce]

The new solid compounds of $A_{3-x}GaO_4H_{1-y}$ (A = Sr, Ba; x ~ 0.15, y ~ 0.3), that is the first oxyhydride containing gallium ion, have been synthesized by high-pressure synthesis. Powder X-ray and neutron diffraction experiments revealed that the series adopts an anti-perovskite structure consisting of hydride-anion-centered HA_6 octahedra with tetrahedral GaO_4 polyanions, wherein the A- and H-sites have partially defected. Formation energy calculation from the raw materials supports that a stoichiometric Ba_3GaO_4H is thermodynamically stable with a wide band gap. Annealing the A = Ba powder under flowing Ar and O_2 gas suggests topochemical H^- desorption and O^{2-}/H^- exchange reactions, respectively.

Introduction

Hydride ions (H^-) in oxides exhibit unique features that are unattainable in other anion species, leading to interesting properties/phenomena.[1] For example, in $SrVO_2H$, almost double compressibility of H^- compared to O^{2-} results in anisotropic lattice shrinkage and deformation under high pressure,[2] while the highly mobile character of H^- in simple perovskite $BaTi(O,H)_3$ enables topochemical anion exchanges to form other mixed-anion compounds such as $BaTi(O,N)_3$ and $BaTi(O,F)_3$.[3, 4] Besides these, a variety of transition metal oxyhydrides (hydride-oxides), e.g. $LaSrCoO_3H_{0.7}$,[5] $ACrO_2H$ (A = Sr, Ba),[6, 7] $LaSr_3NiRuO_4H_4$,[8] hexagonal-$BaTiO_2H$,[9] have been found. Moreover, H^- conduction in oxyhydrides, which consists of electropositive cations including alkali, alkaline-earth, and rare-earth ions, also attracts attention from the perspective of the electrochemical use of hydrogen. By tuning the carrier amount and conduction path in crystal frameworks, fast ionic conduction was achieved in several compounds, such as $La_{2-x-y}Sr_{x+y}LiH_{1-x+y}O_{3-y}$,[10] Ba_2MHO_3 (M = Sc, Y),[11, 12] $Ba_{1.75}LiH_{2.7}O_{0.9}$[13-15], and $LaH_{3-x}O_{x/2}$.[16, 17]

Despite such a rapid growth of oxyhydrides, the use of main group elements (p-block metals) has still been limited, possibly due to the strong reducing property of H^- that easily induces p-block metal deposition. Under such a restriction, the use of polyhedral units like AlO_4 and SiO_4 may become key to expanding the oxyhydride family. One example is $12CaO{\cdot}7Al_2O_3$ mayenite that stabilizes "free hydride ions" in positively charged cages.[18] The cages have reversible hydrogen storage ability, contributing to highly efficient ammonia synthesis.[19, 20] Another cases are A_3AlO_4H (A = Sr, Ba)[21, 22] and Sr_2LiSiO_4H[23, 24] wherein the anionic AlO_4/SiO_4 tetrahedra and H^- ions coexist in the crystal frameworks. The former compounds adopt anti-perovskite structures with a general formula of A_3BX, wherein Ba^{2+} or Sr^{2+}, H^-, and $(AlO_4)^{5-}$ occupy A, B, and X sites, respectively, while the latter compound crystallizes in a monoclinic structure composed of face-shared $(Sr_4Li_2H)^{4+}$ octahedra with isolated $(SiO_4)^{4-}$ units. An oxyhydride series of $Ba_{21}M_2O_5H_{12+x}$ (M = most of p-block metals) contains a suboxide-like cluster $[O_5Ba_{18}]$ consisting of face-shared $[OBa_6]$ octahedra.[25]

Herein, we report a new member of oxyhydrides containing gallium ions. Although hydrogenated intermetallic Zintl phases such as $AGaE$ (A = Ca, Sr, Ba; E = Si, Ge, Sn)[26] and $LaGa_2$[27] have been reported, ionic gallium hydride compounds are almost non-existent or highly unstable, such as GaH_3 (gallane)[28]. Based on the above-mentioned strategy using polyanion units, we successfully synthesized anti-perovskite oxyhydrides $A_{3-x}GaO_4H_{1-y}$ (A = Sr, Ba; **Figure 1**) that are Ga-analogues of A_3AlO_4H by calcination under high pressure. The crystal structures with unique defects in the H-site located at the octahedral center and its anion exchangeability were studied by experiments and calculations.

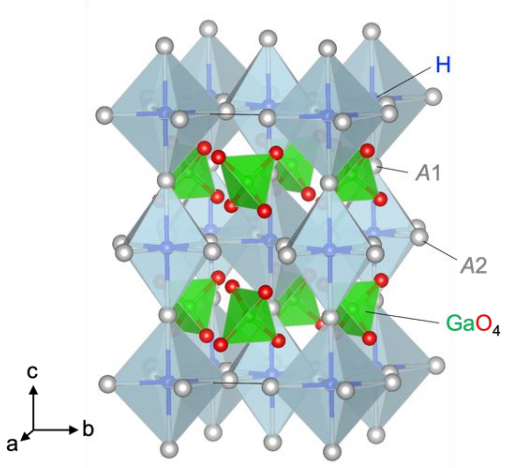

Fig. 1 The crystal structure of A_3GaO_4H (A = Ba, Sr). The green tetrahedral represents

[a] Neutron Science Laboratory (KENS), Institute of Materials Structure Science, High Energy Accelerator Research Organization (KEK), 203-1 Shirakata, Tokai, Ibaraki 319-1106, Japan
[b] SOKENDAI (The Graduate University for Advanced Studies), Shonan Village, Hayama, Kanagawa 240-0193, Japan
[c] Department of Materials Molecular Science, Institute for Molecular Science, 38 Nishigonaka, Myodaiji, Okazaki, Aichi 444-8585, Japan.
[d] PRESTO, Japan Science and Technology Agency (JST), Kawaguchi, Saitama 332-0012, Japan
[e] Solid State Chemistry Laboratory, Cluster for Pioneering Research (CPR), RIKEN, Wako 351-0198, Japan.
E-mail: fumitaka.takeiri@riken.jp; genki.kobayashi@riken.jp
[f] Nanostructures Research Laboratory, Japan Fine Ceramics Center, 2-4-1 Mutsuno, Atsuta-ku, Nagoya 456-8587, Japan
[g] Institute of High Energy Physics, Chinese Academy of Sciences, Beijing, 100049, China
[h] China Spallation neutron source science center, Dongguan, 523803, China

† Footnotes relating to the title and/or authors should appear here.
Electronic Supplementary Information (ESI) available: [details of any supplementary information available should be included here]. See DOI: 10.1039/x0xx00000x

GaO_4. Grey and blue balls represent *A* and H atoms, respectively. Defects in *A*- and H-sites are not considered.

Experimental section

Polycrystalline samples of $A_{3-x}GaO_4H_{1-y}$ (*A* = Sr, Ba) were synthesized by calcination under high pressure. Starting reagents of AH_2 (99.5%, Mitsuwa Chemical Co.), *A*O (99.99%, Aldrich), and Ga_2O_3 (99.99%, Aldrich) were mixed with the molar ratio of 1:5:1 by planetary ball milling using ZrO_2 jar and balls. The deuterated sample was prepared under the same conditions using BaD_2 (Kojundo Chemical) as the deuterium source, replacing BaH_2. In order to prevent loss of hydrogen during reaction, synthesis was carried out under high hydrostatic pressure. The mixture was pressed into pellets with a size of about 4 mm in diameter and sealed in a BN sleeve covered by a NaCl capsule inside a pyrophyllite cell. The cell was pressed under 2 GPa using a cubic anvil apparatus and heated up to 1073 K for 30 minutes before finally quenched to room temperature, followed by gradually releasing the pressure.

As an initial phase characterization, laboratory powder X-ray diffraction (XRD) data were collected using Rigaku MiniFlex 600 with Cu-Kα radiation. Synchrotron X-ray diffraction (SXRD) data were collected at room temperature at BL02B2, SPring-8. Incident beams from a bending magnet were monochromated to λ = 0.419987 or 0.774638 Å. Powder samples were loaded into Pyrex capillaries with an inner diameter of 0.3 mm. The sealed capillary was rotated during the measurements to reduce the effect of the preferred orientation of crystallites. Neutron diffraction (ND) data of Ba_3GaO_4H (310 mg), Ba_3GaO_4D (210 mg), and Sr_3GaO_4D (380 mg) were collected for 12 hours, 8.5 hours, and 8 hours, respectively, at room temperature using a time-of-flight (TOF) diffractometer, SPICA, J-PARC. The sample was mounted in a 6-mm-diameter Ni-V can filled with Ar-gas and the can was rotated during data collection. The crystal structure was refined by the Rietveld analysis using Z–Rietveld software[29, 30] and visualized using the VESTA program.[31] Thermogravimetry (TG) analysis was performed using Rigaku Thermo Plus 8121 with a heating rate of 5 °C/min up to 500 °C under 100 mL/min Ar or O_2 gas flow.

First-principles calculations based on density functional theory (DFT) were performed based on the PAW method as implemented in the VASP code.[32] For the exchange-correlation function, HSE06 functional[33] was used. The applied cut-off energies were 550 eV when lattice constants and internal positions were optimized and 400 eV when only internal positions were optimized. The interval of *k*-point grids was selected to be less than 0.4 $Å^{-1}$ for all perfect cell calculations. Formation energies and densities of intrinsic defects are also evaluated,[34] as described in Supplementary Information.

Results and discussion

Laboratory XRD patterns of the products for the nominal composition of A_3GaO_4H (*A* = Sr, Ba) are shown in **Figure 2**. For *A* = Sr, the majority of reflections can be indexed with a tetragonal unit cell of a = 6.93 Å and c = 11.39 Å, together with reflections assigned to SrO. The tetragonal profile is similar to that of the anti-perovskite Sr_3AlO_4H oxyhydride (*I*4/*mcm*: a = 6.7560 Å, c = 11.1567 Å), wherein the corner-shared HSr_6 octahedra form a three-dimensional framework with the tetrahedral AlO_4 polyanions at the channels surrounded by the eight octahedra[22]. For *A* = Ba, a similar tetragonal phase with the larger lattice constants of a = 7.33 Å and c = 11.73 Å was obtained in nearly a single phase. These results indicate a successful preparation of new anti-perovskite oxyhydrides containing GaO_4 polyanion units. Both powder products were grey in colour, suggesting the presence of a tiny amount of gallium metal or/and compound with reduced gallium ion species as an unidentified minor phase. When the product for *A* = Ba was exposed to air, it decomposed immediately (**Figure S1**).

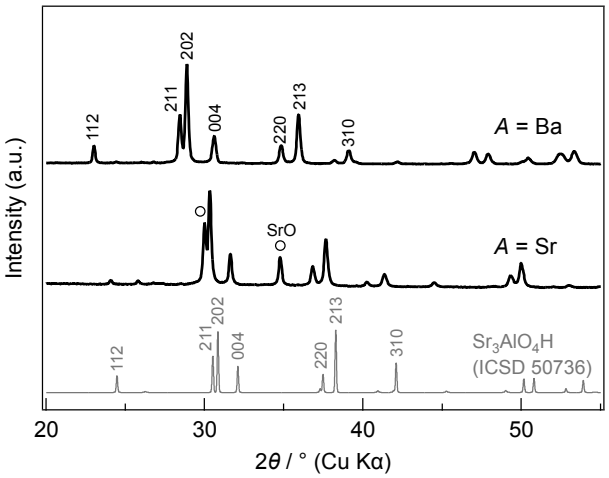

Fig. 2 Powder XRD pattern of the products for the nominal compositions of A_3GaO_4H (*A* = Sr, Ba) prepared by high-pressure synthesis, together with the simulated pattern of Sr_3AlO_4H (gray line)[22].

Synchrotron X-ray diffraction (SXRD) experiments were carried out for both *A* = Sr and Ba products. We performed refinements assuming structure models that were constructed referring to Sr_3AlO_4H[22]. Hydrogen species were not considered here, and a secondary phase of SrO was added for *A* = Sr. Given that tetrahedral MO_4 polyanions (*M* = Al, Si, P, Ga, etc.) are robust units in general, the occupancy factors of Ga and O, g(Ga) and g(O), were fixed at unity in the following analysis. Refinements converged well, as shown in **Figure 3**, and the detailed crystal parameters are summarized in **Table S1**. The occupancy factors of *A*1 site, g(*A*1), were refined as 0.92916(6) for *A* = Ba and 0.9219(5) for *A* = Sr, while no significant deficiency was detected at the *A*2 site for both cases. Note that the refined isotropic displacement parameters of the *A*1 sites are relatively large at 1.33 and 0.892 for Ba and Sr species, respectively. This tendency is similar to that observed for isostructural compounds such as Sr_3AlO_4H[22] and Sr_3GaO_4F[35], although a deficiency in *A*1 sites has not been pointed out in previous works.

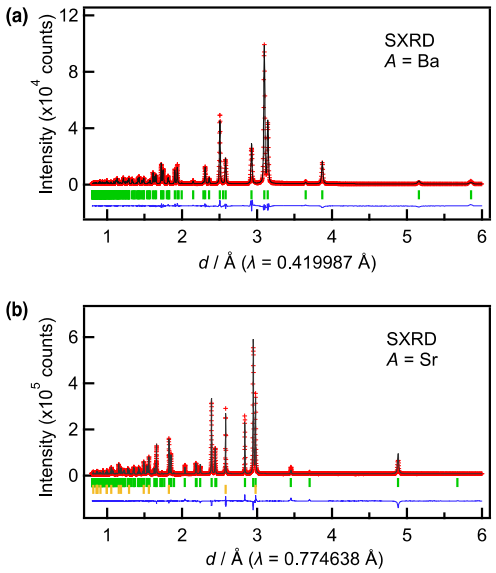

Fig. 3 SXRD pattern of (a) Ba_3GaO_4H and (b) Sr_3GaO_4H. The red points and black curve indicate the observed and calculated intensities, respectively. The blue line shows the differential curve between the observed and calculated patterns, the green lines and yellow indicate the positions of the Bragg reflections of the main phase and the impurity of SrO, respectively.

In order to obtain information regarding the hydrogen species, powder neutron diffraction (ND) experiments were performed for both hydride/deuteride products of *A* =Ba. The contribution of incoherence scattering derived from hydrogen species appeared as a higher background level. The differences in the relative peak intensity (**Figure S2**) strongly support the presence of H/D species in the anti-perovskite, as seen in 202 peaks as represented for *A* = Ba (**Figure 4b**). We refined the profiles of hydride and deuteride samples for *A* = Ba using the structural model based on the result of X-ray refinement, wherein H/D atoms were added at Wyckoff position 4*c* (0,0,0). Occupancies of *g*(Ba1) and *g*(D) were refined as independent variables, while the others were fixed as unity. The refinements converged well, as shown in **Figure 4a**, and the refined parameters are summarized in **Table 1** for the deuteride sample with a composition of $Ba_{2.85}GaO_4D_{0.70}$, while the refinement results of the hydride sample are shown in **Figure S3** and **Table S2** with the composition of $Ba_{2.8}GaO_4H_{0.7}$. The ND profiles of *A* = Sr were also refined, yielding $Sr_{2.93}GaO_4D_{0.76}$ (**Figure S4** and **Table S3**). These results indicate the presence of defects at the *A*- and H-sites with the general formula $A_{3-x}GaO_4H_{1-y}$. As for *A* = Ba, the defect manner seems Schottky-like coupled with A^{2+} and $2H^-$ in charge neutrality. It should be noted that some H^- conducting materials include intrinsic Schottky-like deficiencies, e.g. $Ba_{2-\delta}H_{3-2\delta}X$ (*X* = Cl, Br, I; $\delta \sim 0.15$-0.3)[36] and $Ba_{2-x-y}LiH_{3-2x}O_{1-y}$ ($x \sim 0.15$, $y \sim 0.1$)[13].

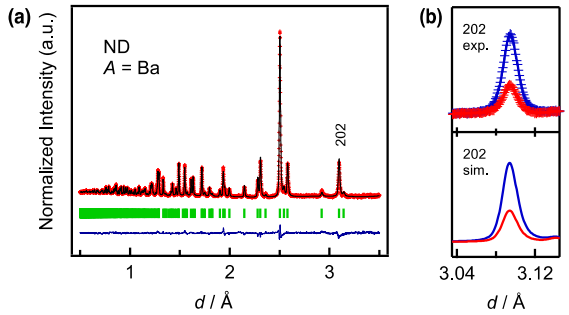

Fig. 4 (a) Rietveld refinement of the powder ND pattern of $Ba_{3-x}GaO_4D_{1-y}$ at room temperature. The red points and black curves indicate the observed and calculated intensities, respectively. The blue line shows the differential curve between the observed and calculated patterns, the green lines indicate the positions of the Bragg reflections of the main phase. (b) The magnification of 202 peaks observed experimentally (top) and simulated with the H/D occupancy of 0.7 (bottom). The blue line and points represent H case, and the red line and points represent D case.

Table 1 Crystal structure parameters of $Ba_{3-x}GaO_4D_{1-y}$ obtained from Rietveld refinement of room temperature ND data.

atom	site	*g*	*x*	*y*	*z*	*B*/Å²
Ba1	4*a*	0.8496(14)	0	0	1/4	0.78(2)
Ba2	8*h*	1	0.17489(6)	0.67489(6)	0	0.19(1)
Ga1	4*b*	1	0	1/2	1/4	0.24(1)
D1	4*c*	0.699(3)	0	0	0	1.45(3)
O2	16*l*	1	0.13914(4)	0.63914(4)	0.65098(4)	1.13(1)

Unit cell: Tetragonal *I*4/*mcm*; $a = b = 7.29261(4)$Å, $c = 11.68652(10)$Å, $S = 1.67$, $R_{wp} = 2.44\%$, $R_p = 2.07\%$, $R_e = 1.46\%$, $R_B = 5.39\%$, $R_F = 5.60\%$.

Table 2 summarizes the bond valence sum (BVS) values calculated from the refined structures of the ND data. The values obtained for *A*2 and Ga were approximately +2 and +3, respectively, which agreed well with the formal charges of A^{2+} and Ga^{3+}. In contrast, the values for *A*1, +1.32 for Ba1, and +1.20 for Sr1 are smaller than the expected +2, meaning that they are under-bonding states. The under-bonding state of the *A*1 (4*a*) site was reported in other isostructural compounds with values of ~1.3 for Sr_3GaO_4F[37] and Sr_3AlO_4H[22], and ~1.4 for $LaSr_2AlO_5$.[38] In $LaSr_2AlO_5$, the under-bonding of the 4*a* site was reported due to the distribution of Sr-O observed in the pair distribution analysis[38]. BVS calculations for H and O give values that are slightly larger and smaller than the expected –1 and –2, respectively, although the origin of this trend is unknown. Note that refinements assuming H/O site mixing resulted in no improvement in fitting.

Table 2 Bond valence sum of A_3GaO_4D calculated from ND data.

atom	site	bond valence sum	
		A = Ba (D)	*A* = Sr (D)
(Ba,Sr)1	4*a*	1.32	1.20
(Ba,Sr)2	8*h*	2.15	2.04
Ga1	4*b*	2.94	3.06
D1	4*c*	1.42	1.14
O1	16*l*	1.78	1.80

The obtained new gallium oxyhydride was also studied using DFT calculations. We evaluated the formation energy ΔE_f of stoichiometric "Ba_3GaO_4H" from the raw materials of β-Ga_2O_3,

NaCl-type BaO, and $PbCl_2$-type BaH_2. Calculations gave ΔE_f = −138.84 kJ/mol, showing that the anti-perovskite Ba_3GaO_4H is thermodynamically stable. The calculated lattice parameters of a = 7.2448 Å and c = 11.8021 Å were close to the experimental values with relative errors of –0.66% and +0.99%, respectively. **Figure 5** shows the orbital-dependent density of states of each atom in Ba_3GaO_4H. While the valence band maximum (VBM) is composed of O-2p, H-1s, and *p* and *d* orbitals of cations, the conduction band minimum is mainly composed of Ba-*d* orbitals. This verifies that the 1*s* orbitals of H are occupied. The calculated bandgap of the material was 5.28 eV. From the large gap, we can expect that the crystals are transparent when such a stoichiometric composition was prepared in a single phase, though prepared samples are not in most cases. Note that, we also calculated the formation energies and related densities of isolated point defects in the crystal, but the results were inconsistent with the experimental results in the manner of Ba deficiency (details are provided in Supplementary Information).

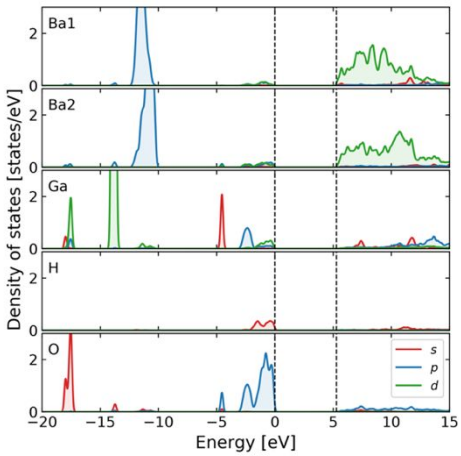

Fig. 5 Density of states (DOS) of each orbital of each atom in Ba_3GaO_4H crystal, where the energy is measured from the valence band maximum and DOS are smeared using a Gaussian function with the width of 0.1 eV.

The newly synthesized gallium oxyhydrides can be categorized as new members of A_3MO_4X (*A* = Sr, Ba; *M* = Al, Ga; *X* = H, F) mixed-anion anti-perovskites. In comparison with the oxyhydrides (*X* = H), the larger GaO_4 tetrahedra rather than AlO_4 give impact on the HA_6 octahedral tilting manner. The Ga-series for both *A* = Sr and Ba adopts tetragonal unit cells (*I*4/*mcm*) with the point-shared HA_6 octahedra along *c*-axis in straight (∠H-*A*1-H = 180°; see Figure 1). The same symmetry was also reported for Sr_3AlO_4H, whereas Ba_3AlO_4H adopts a distorted orthorhombic cell (*Pnma*) with buckled HBa_6 octahedra[21]. We calculated the Goldschmidt tolerance factor *t*, which is typically used to discuss the stability of the perovskite structure[39], for the four A_3MO_4H anti-perovskite series, yielding 0.929-0.948 for the tetragonal class, and 0.916, the furthest from unity, for orthorhombic Ba_3AlO_4H (Table S4).

The difference in the *X* site, i.e., oxyhydride *vs.* oxyfluoride, also provides an interesting insight. Oxyfluorides of A_3AlO_4F and A_3GaO_4F were well studied as phosphor materials,[22, 35] however, there is no report for pure *A* = Ba members like "Ba_3AlO_4F" and "Ba_3GaO_4F".[40] This trend may be derived from the somewhat large ionic radius of Ba^{2+} (1.35 Å with the coordination number of 6) for the vertex position of the FA_6 octahedra. In contrast, oxyhydrides of orthorhombic Ba_3AlO_4H[21] and tetragonal Ba_3GaO_4H (this work) are both stable, possibly owing to the size flexibility (tolerance) of hydride ion[41].

Sizable defects in hydrogen at the octahedral center in $A_{3-x}GaO_4H_{1-y}$ have not been reported in the A_3MO_4X series, as far as we know. This non-stoichiometric nature may allow topochemical reactions via ion diffusion. Thermogravimetry (TG) result of $Ba_{2.85}GaO_4H_{0.7}$ in heating under Ar gas flow, showed nearly no mass change, while the XRD pattern after TG showed a significant peak shift toward a higher angle that corresponds to lattice shrinkage (**Figure 6**), suggesting hydrogen release from the anti-perovskite framework. In contrast, TG under O_2 gas flow exhibited ~2% mass gain, together with a peak shift toward a lower angle in XRD, together with broadening the profile. This result indicates that topochemical O^{2-}/H^- substitution occurred, and the composition of $Ba_{2.85}GaO_{4+\delta}$ (δ ~ 0.7) was obtained. Given that this type of structure, wherein oxygen species are located at the octahedral center in anti-perovskite, was reported in oxide-ion-conducting $BaLa_2ZnO_5$[42], partial oxygen occupancy after anion exchange may potentially enhance the oxide ion diffusivity. The highly mobile and anion-exchangeable property of H^- was reported in regular perovskite oxyhydride $BaTiO_{3-x}H_x$ with H^- ions at the vertex position,[43, 44] it is interesting in our case that such a property could appear even in H^- at the octahedral center. This nature might be rather close to that of $12CaO{\cdot}7Al_2O_3$ mayenite with exchangeable H^- ions in the positively charged cages.

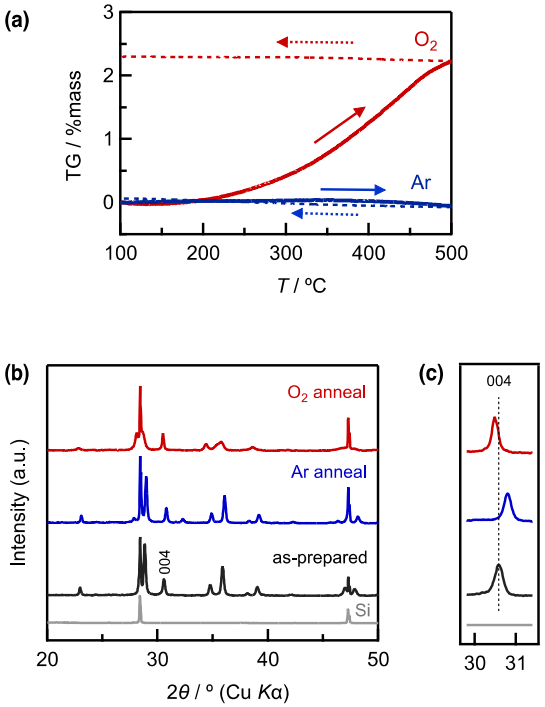

Fig. 6 (a) TG curve of the sample *A* = Ba during heating (solid line) and cooling (dotted line) under O_2-gas flow (red lines) and Ar-gas flow (blue lines). (b) XRD pattern of the sample *A*=Ba before and after TG-measurement. The gray, and black curves represent the observed intensities of Si and the as-prepared sample. The blue and red curves indicate the observed intensities of Ar annealed and O2 annealed samples, respectively.

Conclusions

A new member of the p-block metal oxyhydrides $A_{3-x}GaO_4H_{1-y}$ (A = Sr, Ba) was successfully obtained by high-pressure synthesis. Powder X-ray and neutron diffraction study revealed that this series adopts an iso-structure of Sr_3AlO_4H with unique defects at A- and H-sites. The formation energy calculation from the raw materials supported that stoichiometric "Ba_3GaO_4H" is thermodynamically stable with a wide band gap of 5.28 eV. Hydride ions at the octahedral center could be topochemically desorbed or exchanged by sintering under Ar or O_2 gas flow. Recently, hydride-based anti-perovskites with polyanion units are expanding, e.g. transition-metal oxometallate hydride A_3MO_4H (A = Rb, Cs; M = Mo, W)[45] and largely octahedral distorted $Na_3(ZnH_4)H$[46]. In the future, other p-block metal polyanions, such as GeO_4 and InO_4 units, could also be used as building blocks in hydride compounds, possibly leading to new functional materials including ion conductors and catalysis.

Conflicts of interest

There are no conflicts to declare.

Acknowledgements

This work was supported by JSPS, KAKENHI (JP16H06440, JP18H05516, JP19H04710, JP20H02828, JP22K14755, JP22H04514, JP22H05146, JP22K18909), and JST, PRESTO (JPMJPR20T2), FOREST (JPMJFR213H). The synchrotron radiation experiments were performed at BL02B2 of SPring-8, with the approval of the Japan Synchrotron Radiation Research Institute (JASRI) (2019A1084). The neutron experiments were conducted at J-PARC (2019S10).

References

1. H. Kageyama, K. Hayashi, K. Maeda, J. P. Attfield, Z. Hiroi, J. M. Rondinelli and K. R. Poeppelmeier, *Nat Commun*, 2018, **9**, 772.
2. T. Yamamoto, D. Zeng, T. Kawakami, V. Arcisauskaite, K. Yata, M. A. Patino, N. Izumo, J. E. McGrady, H. Kageyama and M. A. Hayward, *Nat Commun*, 2017, **8**, 1217.
3. T. Yajima, F. Takeiri, K. Aidzu, H. Akamatsu, K. Fujita, W. Yoshimune, M. Ohkura, S. Lei, V. Gopalan, K. Tanaka, C. M. Brown, M. A. Green, T. Yamamoto, Y. Kobayashi and H. Kageyama, *Nat Chem*, 2015, **7**, 1017-1023.
4. Y. Kobayashi, O. J. Hernandez, T. Sakaguchi, T. Yajima, T. Roisnel, Y. Tsujimoto, M. Morita, Y. Noda, Y. Mogami, A. Kitada, M. Ohkura, S. Hosokawa, Z. Li, K. Hayashi, Y. Kusano, J. Kim, N. Tsuji, A. Fujiwara, Y. Matsushita, K. Yoshimura, K. Takegoshi, M. Inoue, M. Takano and H. Kageyama, *Nat Mater*, 2012, **11**, 507-511.
5. M. A. Hayward, E. J. Cussen, J. B. Claridge, M. Bieringer, M. J. Rosseinsky, C. J. Kiely, S. J. Blundell, I. M. Marshall and F. L. Pratt, *Science*, 2002, **295**, 1882-1884.
6. C. Tassel, Y. Goto, Y. Kuno, J. Hester, M. Green, Y. Kobayashi and H. Kageyama, *Angew Chem Int Ed Engl*, 2014, **53**, 10377-10380.
7. K. Higashi, M. Ochi, Y. Nambu, T. Yamamoto, T. Murakami, N. Yamashina, C. Tassel, Y. Matsumoto, H. Takatsu, C. M. Brown and H. Kageyama, *Inorg Chem*, 2021, **60**, 11957-11963.
8. L. Jin, M. Lane, D. Zeng, F. K. K. Kirschner, F. Lang, P. Manuel, S. J. Blundell, J. E. McGrady and M. A. Hayward, *Angew Chem Int Ed Engl*, 2018, **57**, 5025-5028.
9. M. Miyazaki, K. Ogasawara, T. Nakao, M. Sasase, M. Kitano and H. Hosono, *Journal of the American Chemical Society*, 2022, **144**, 6453-6464.
10. G. Kobayashi, Y. Hinuma, S. Matsuoka, A. Watanabe, M. Iqbal, M. Hirayama, M. Yonemura, T. Kamiyama, I. Tanaka and R. Kanno, *Science*, 2016, **351**, 1314 - 1317.
11. F. Takeiri, A. Watanabe, A. Kuwabara, H. Nawaz, N. I. P. Ayu, M. Yonemura, R. Kanno and G. Kobayashi, *Inorg. Chem.*, 2019, **58**, 4431-4436.
12. H. Nawaz, F. Takeiri, A. Kuwabara, M. Yonemura and G. Kobayashi, *Chem. Commun.*, 2020, **56**, 10373-10376.
13. F. Takeiri, A. Watanabe, K. Okamoto, D. Bresser, S. Lyonnard, B. Frick, A. Ali, Y. Imai, M. Nishikawa, M. Yonemura, T. Saito, K. Ikeda, T. Otomo, T. Kamiyama, R. Kanno and G. Kobayashi, *Nat Mater*, 2022, **21**, 325-330.
14. K. Okamoto, F. Takeiri, Y. Imai, M. Yonemura, T. Saito, K. Ikeda, T. Otomo, T. Kamiyama and G. Kobayashi, *J. Mater. Chem. A*, 2022, **10**, 23023-23027.
15. K. Okamoto, F. Takeiri, Y. Imai, M. Yonemura, T. Saito, K. Ikeda, T. Otomo, T. Kamiyama and G. Kobayashi, *Advanced Science*, 2023, **10**, 2203541.
16. K. Fukui, S. Iimura, T. Tada, S. Fujitsu, M. Sasase, H. Tamatsukuri, T. Honda, K. Ikeda, T. Otomo and H. Hosono, *Nat Commun*, 2019, **10**, 2578.
17. K. Fukui, S. Iimura, A. Iskandarov, T. Tada and H. Hosono, *J Am Chem Soc*, 2022, **144**, 1523-1527.
18. K. Hayashi, S. Matsuishi, T. Kamiya, M. Hirano and H. Hosono, *Nature*, 2002, **419**, 462.
19. Y. Inoue, M. Kitano, M. Tokunari, T. Taniguchi, K. Ooya, H. Abe, Y. Niwa, M. Sasase, M. Hara and H. Hosono, *ACS Catalysis*, 2019, **9**, 1670-1679.
20. M. Kitano, S. Kanbara, Y. Inoue, N. Kuganathan, P. V. Sushko, T. Yokoyama, M. Hara and H. Hosono, *Nat Commun*, 2015, **6**, 6731.
21. B. Huang and J. D. Corrbet, *Journal of Solid State Chemistry*, 1998, **141**, 570-575.
22. T. Wu, K. Fujii, T. Murakami, M. Yashima and S. Matsuishi, *Inorg Chem*, 2020, **59**, 15384-15393.
23. F. Gehlhaar, R. Finger, N. Zapp, M. Bertmer and H. Kohlmann, *Inorg. Chem.*, 2018, **57**, 11851-11854.
24. T. Wu, A. Ishikawa, T. Honda, H. Tamatsukuri, K. Ikeda, T. Otomo and S. Matsuishi, *RSC Advances*, 2019, **9**, 5282-5287.
25. M. Jehle, A. Hoffmann, H. Kohlmann, H. Scherer and C. Röhr, *J. Alloys Compd.*, 2015, **623**, 164-177.
26. M. J. Evans, G. P. Holland, F. J. Garcia-Garcia and U. Häussermann, *Journal of the American Chemical Society*, 2008, **130**, 12139-12147.
27. A. Werwein, C. Benndorf, M. Bertmer, A. Franz, O. Oeckler and H. Kohlmann, *Crystals*, 2019, **9**, 193.
28. A. J. Downs, M. J. Goode and C. R. Pulham, *Journal of American Chemical Society*, 1989, **111**, 1936–1937.
29. R. Oishi, M. Yonemura, Y. Nishimaki, S. Torii, A. Hoshikawa, T. Ishigaki, T. Morishima, K. Mori and T. Kamiyama, *Nuclear Instruments and Methods in Physics Research Section A: Accelerators, Spectrometers, Detectors and Associated Equipment*, 2009, **600**, 94-96.

30. R. Oishi-Tomiyasu, M. Yonemura, T. Morishima, A. Hoshikawa, S. Torii, T. Ishigaki and T. Kamiyama, *Journal of Applied Crystallography*, 2012, **45**, 299-308.
31. K. Momma and F. Izumi, *Journal of Applied Crystallography*, 2008, **41**, 653-658.
32. G. Kresse and D. Joubert, *Physical Review B*, 1999, **59**, 1758 - 1775.
33. J. Heyd, G. E. Scuseria and M. Ernzerhof, *The Journal of Chemical Physics*, 2003, **118**, 8207-8215.
34. C. Freysoldt, B. Grabowski, T. Hickel, J. Neugebauer, G. Kresse, A. Janotti and C. G. Van de Walle, *Reviews of Modern Physics*, 2014, **86**, 253-305.
35. R. L. Green, M. Avdeev and V. Pierre, *Journal of Solid State Chemistry*, 2019, **276**, 376-381.
36. H. Ubukata, F. Takeiri, K. Shitara, C. Tassel, T. Saito, T. Kamiyama, T. Broux, A. Kuwabara, G. Kobayashi and H. Kageyama, *Science Advances*, 2021, **7**, eabf7883.
37. T. Vogt, P. M. Woodward, B. A. Hunter, A. K. Prodjosantoso and B. J. Kennedy, *J. Solid State Chem.*, 1999, **144**, 228-231.
38. W. B. Im, K. Page, S. P. DenBaars and R. Seshadri, *Journal of Materials Chemistry*, 2009, **19**.
39. V. V. M. Goldschmidt, *Naturwissenschaften*, 1926, **14**, 477–485.
40. R. L. Green, *thesis, University of South Carolina*, 2013.
41. H. Ubukata, T. Broux, F. Takeiri, K. Shitara, H. Yamashita, A. Kuwabara, G. Kobayashi and H. Kageyama, *Chem. Mater.*, 2019, **31**, 7360-7366.
42. K. Nakamura, K. Fujii, E. Niwa and M. Yashima, *Journal of the Ceramic Society of Japan*, 2018, **126**, 292-299.
43. T. Yajima, F. Takeiri, K. Aidzu, H. Akamatsu, K. Fujita, W. Yoshimune, M. Ohkura, S. Lei, V. Gopalan, K. Tanaka, C. M. Brown, M. A. Green, T. Yamamoto, Y. Kobayashi and H. Kageyama, *Nat Chem*, 2015, **7**, 1017-1023.
44. N. Masuda, Y. Kobayashi, O. Hernandez, T. Bataille, S. Paofai, H. Suzuki, C. Ritter, N. Ichijo, Y. Noda, K. Takegoshi, C. Tassel, T. Yamamoto and H. Kageyama, *J. Am. Chem. Soc.*, 2015, **137**, 15315-15321.
45. A. Mutschke, A. Schulz, M. Bertmer, C. Ritter, A. J. Karttunen, G. Kieslich and N. Kunkel, *Chem Sci*, 2022, **13**, 7773-7779.
46. S. Gao, C. Tassel, S. Fujii, H. Ubukata, T. Zhu, D. Zhang, T. Broux, T. Saito, C. Zhong, E. Yoruk, K. Yamamoto, A. Kuwabara, Y. Uchimoto and H. Kageyama, *Chemistry of Materials*, 2022, **34**, 6815-6823.